Radiation Oncology

RESEARCH Open Access

A multifunctional targeted nano-delivery system with radiosensitization and immune activation in glioblastoma

Xin Wen[1,2,4†], Zhiying Shao[1†], Xueting Chen[1†], Hongmei Liu[3], Hui Qiu[2], Xin Ding[2,4], Debao Qu[1,2], Hui Wang[1], Andrew Z. Wang[4*] and Longzhen Zhang[1,2,5*]

Abstract

Glioblastoma (GBM), the most common primary brain malignancy in adults, is notoriously difficult to treat due to several factors: tendency to be radiation resistant, the presence of the blood brain barrier (BBB) which limits drug delivery and immune-privileged status which hampers effective immune responses. Traditionally, high-dose irradiation (8 Gy) is known to effectively enhance anti-tumor immune responses, but its application is limited by the risk of severe brain damage. Currently, conventional dose segmentation (2 Gy) is the standard radiotherapy method, which does not fully exploit the potential of high-dose irradiation for immune activation. The hypothesis of our study posits that instead of directly applying high doses of radiation, which is risky, a strategy could be developed to harness the immune-stimulating benefits of high-dose irradiation indirectly. This involves using nanoparticles to enhance antigen presentation and immune responses in a safer manner. Angiopep-2 (A2) was proved a satisfactory BBB and brain targeting and Dbait is a small molecule that hijack DNA double strand break damage (DSB) repair proteins to make cancer cells more sensitive to radiation. In view of that, the following two nanoparticles were designed to combine immunity of GBM, radiation resistance and BBB innovatively. One is cationic liposome nanoparticle interacting with Dbait (A2-CL/Dbait NPs) for radiosensitization effect; the other is PLGA-PEG-Mal nanoparticle conjugated with OX40 antibody (A2-PLGA-PEG-Mal/anti-OX40 NPs) for tumor-derived protein antigens capture and optimistic immunoregulatory effect of anti-OX40 (which is known to enhance the activation and proliferation T cells). Both types of nanoparticles showed favorable targeting and low toxicity in experimental models. Specifically, the combination of A2-CL/Dbait NPs and A2-PLGA-PEG-Mal/anti-OX40 NPs led to a significant extension in the survival time and a significant tumor shrinkage of mice with GBM. The study demonstrates that combining these innovative nanoparticles with conventional radiotherapy can effectively address key challenges in GBM treatment. It represents a significant step toward more effective and safer therapeutic options for GBM patients.

†Xin Wen, Zhiying Shao and Xueting Chen contributed equally to this work.

*Correspondence:
Andrew Z. Wang
Andrew.Wang2@UTSouthwestern.edu
Longzhen Zhang
jsxyfyzlz@126.com

Full list of author information is available at the end of the article

Keywords Glioblastoma, Blood brain barrier (BBB), Immune, Radiosensitization, OX40, Nanoparticle

Introduction

Glioblastoma (GBM) is the most common primary brain malignancy in adults. The primary challenges in GBM therapy including radiation resistance, blood brain barrier (BBB) and immune privilege of central nervous system (CNS). These factors contribute to high postoperative recurrence and poor therapeutic efficacy. And addressing these issues is crucial for improving GBM treatment outcomes [1–4].

Radiation resistance, whether innate or acquired, significantly impairs the efficacy of radiotherapy in treating GBM. Radiotherapy, a primary cancer treatment modality, works by inducing DNA double-strand breaks (DSBs) in cancer cells to promote cancer cell death. Dbait, a 32 base-pair deoxyribonucleotides double-stranded DNA molecule, acts as a "bait" to mimic the ends of DSBs, thereby recruiting DSB repair proteins and enzymes [5, 6]. Consequently, the failed timely DSB repair led to inevitable death of cancer cells due to insufficient recruitment of DNA damage repair factors, resulting in the improvement of GBM cells radiation sensitivity. In previous study, we have reported Dbait can sensitize prostate cancer cells to radiation treatment [7]. However, when applied intravenously, Dbait is rapidly degraded by DNase, limiting its effectiveness. Although modifications, such as cholesterol conjugation, have been employed to protect Dbait from degradation by liver and kidney metabolism [8], these alterations result in a relatively large, negatively charged molecule with poor targeting ability to GBM sites [9, 10]. An ideal vector for Dbait delivery should be carefully engineered to efficiently cross the BBB and specifically target GBM cells when injected via the tail vein.

Cationic liposomes are bilayer lipid molecules composed of positively charged cationic lipids and neutral phospholipids, which are widely used in drug delivery due to their positive charge, high transfection efficiency, low toxicity, easy modification of target head, and electrostatic interaction with cell membrane [11–14]. The positive charge of cationic liposomes allows for effective electrostatic interactions with negatively charged molecules like Dbait.

However, cationic liposomes alone face limitations in penetrating the BBB due to the lack of targeting. Angiopep-2 (A2), a 24 kDa peptide consisting of 19 amino acids, serves as a ligand for low-density lipoprotein receptor-related protein-1 (LRP-1). A2 was proved to target BBB and GBM expressing LRP-1, thereby addressing the targeting limitations of cationic liposomes [11, 15–17]. To enhance the effectiveness of Dbait delivery, Dbait-loaded cationic liposome nanoparticles have been modified with A2. This modification aims to improve targeting to GBM cells, overcome BBB penetration challenges, and mitigate the risk of radioresistance, thereby optimizing the therapeutic potential of radiotherapy in GBM treatment.

The combination of radiotherapy and immunotherapy, particularly with immune checkpoint inhibitors (ICIs), has significantly advanced cancer treatment. Among the targets in cancer immunotherapy, OX40 (CD134, TNFRSF4) stands out. OX40 is a type I transmembrane glycoprotein belonging to the tumor necrosis factor receptor (TNFR) superfamily [18]. OX40 is mainly expressed on activated effector T cells (Teffs) and regulatory T cells (Tregs) and plays a crucial role by promoting Teffs activation and inhibiting Tregs [18]. OX40L, the ligand of OX40, is predominantly found on activated antigen presenting cells (APCs) [18]. The binding of OX40 and OX40L is a significant costimulatory signal and strengthens the immune response. For example, a 2018 animal study by SagIV-Barfi I. et al. showed that intratumoral injection of CpG combined with anti-OX40 antibodies promoted local tumor regression and immunological distancing effect [19]. However, the efficacy of OX40-targeted immunotherapy is contingent upon the presence of sufficient tumor-specific T cells. In malignancies characterized by extensive invasion and weak immunogenicity, the lack of activated tumor-specific T cells poses a challenge to achieving effective immunoregulation with anti-OX40 therapy [20].

Currently, high-dose irradiation (8 Gy) was confirmed to be the optimal dose to stimulate anti-tumor immune response. However, this dose is rarely applied in GBM radiotherapy due to the risk of significant radiation-induced brain damage. Conventional dose segmentation (2 Gy) is still the standard approach in radiotherapy. We assume that by enriching and presenting a small amount of antigens generated under conventional dose irradiation, it may be possible to achieve immune responses similar to those induced by 8 Gy radiation. Our previous study has reported various antigen-capturing nanoparticles (AC-NPs) that can capture tumor-derived protein antigens (TDPAs), which were prepared by discrepant surface modification methods and use biodegradable polylactic acid-glycolic acid copolymer as the core [21]. PLGA AC-NPs and PLGA-PEG-Mal AC-NPs were detected to have the strongest ability to capture TDPAs, promoting the activation and expansion of $CD8^+$ T cells via antigen presentation of APCs, resulting in immune-enhancing and immunological remote effects. Mi Y. et al. prepared a dual immunotherapy NP by conjugating anti-OX40 and anti-PD-1 to PEG-PLGA AC-NPs, which contributed to optional T-cell activation and effective

cancer immunotherapy [22]. Building on these findings, we designed PLGA-PEG-Mal NPs conjugated with anti-OX40 and modified with A2. This formulation aims to capture TDPAs and activate T cells, with the goal of enhancing the therapeutic efficacy of anti-OX40 therapy in GBM.

Based on our previous research and the findings outlined, we have developed two innovative nanoparticles designed to address GBM's immune evasion, radiation resistance, and the challenges of crossing the blood-brain barrier (BBB) (Fig. 1). One is cationic liposome NPs which are engineered to interact with Dbait, enhancing radiosensitization effects in GBM cells. The cationic liposomes facilitate effective delivery of Dbait, improving the efficacy of radiotherapy by promoting the accumulation of DNA damage and enhancing the sensitivity of GBM cells to radiation. The other is PLGA-PEG-Mal NPs which are conjugated with anti-OX40 antibodies to capture TDPAs and provide an immunoregulatory effect. Both types of NPs are modified with A2 to enable penetration through the BBB and to specifically target GBM cells, thereby addressing the challenges associated with delivering therapeutic agents to brain tumors.

Materials and methods

Cell lines and Dbait molecule

G422 (G422 was firstly induced astrocytoma by implanting methylcholanthracene in the brain of KM mice, which were then transformed into glioblastoma in the 120th generation. G422 cells were epithelial-like) and GL261 (GL261 were also induced by intracranial injection of 3-methylcholanthracene into C57BL/6 mice, which were fibroblast-like) cells were kindly provided by Cell Bank, Chinese Academy of Sciences and were cultured in completed DMEM medium (Sigma, D5796) with 10% fetal bovine serum (FBS) (Ever Green, 11011−8611) and 1% penicillin and streptomycin (Beyotime, C0222). LO_2 cells were granted from Xuzhou Medical University. The sequence of Dbait (Genscript Biotechnology, China) were: 5'-GCTGTGCCCACAACCCAGCAAACAAGCC TAGA-(H)-TCTAGGCTTGTTTGCTGGGTTGTGGG CACAGC-3', where H was a hexaethylene glycol linker. The sequence of Cy3-siRNA used for targeting is: 5'-UUC UCC GAA CGU GUC ACG UTT-3'; 3'-ACG UGA CAC GUU CGG AGA ATT-5'.

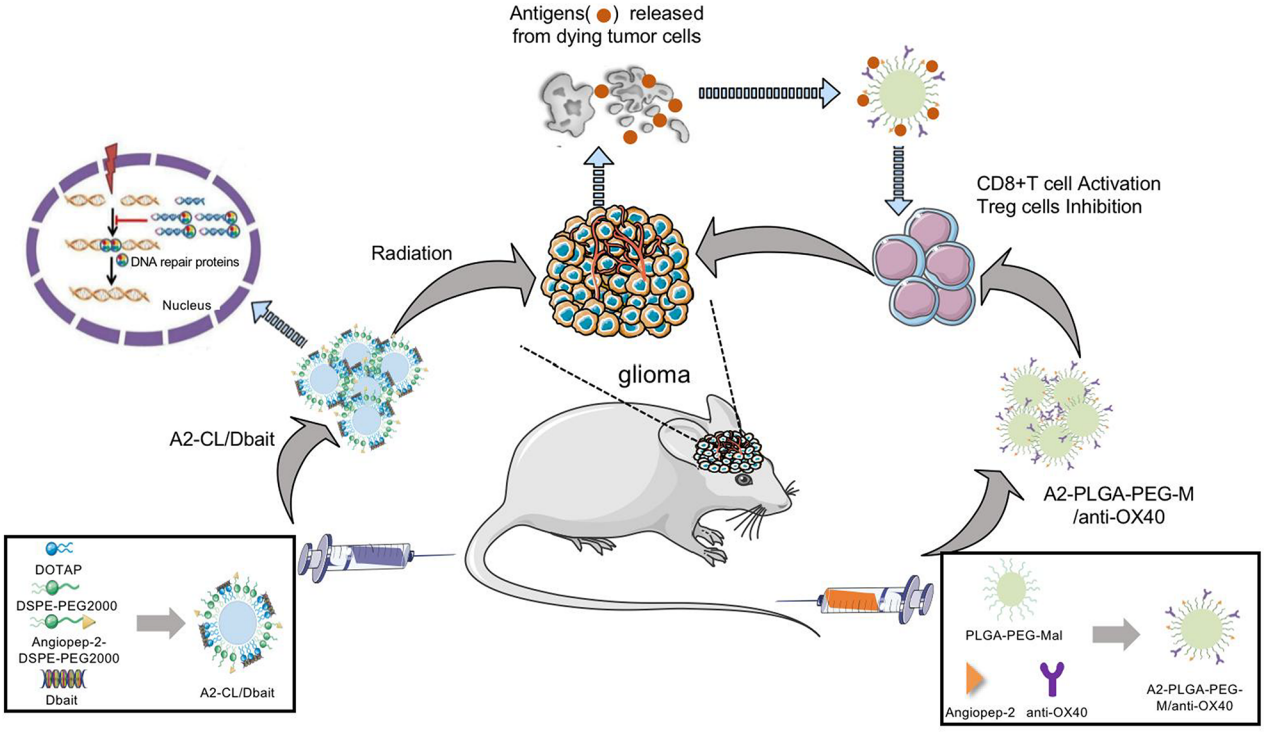

Fig. 1 Schematic depicting the progress of two nanoparticles enhancement of anti-GBM by the combination radiation sensitivity and immunotherapy. Cationic liposome NPs which are engineered to interact with Dbait, enhancing radiosensitization effects by promoting the accumulation of DNA damage in GBM cells. PLGA-PEG-Mal NPs which are conjugated with anti-OX40 antibodies are engineered to capture TDPAs and provide a costimulator of T-cell activation effect. Both types of NPs are modified with A2 to enable penetration through the BBB and to specifically target GBM cells, thereby addressing the challenges associated with delivering therapeutic agents to brain tumors. GBM: giloma; NPs: nanoparticles; A2: Angiopep2; TDPAs: tumor derived protein antigens

Preparation and characterization of nanoparticles

Cationic liposome NPs interacting with Dbait was prepared as previously described [23, 24]. Briefly, DOTAP (AVT, O01004), DOPC (AVT, B80378), cholesterol (AVT, B61251), DSPE-PEG2000 (AVT, 20490214), DSPE-PEG2000-Angiopep-2 were mixed in a molar ratio of 40:10:40:9.5:0.5. The mixture was slowly dropped into aqueous phase with the oil to water ratio of 3:7, and the total volume was 1 ml. The mixed solution was loaded in a dialysis bag and immersed in 3 L DEPC for 2 h, which was then collected as cationic liposomes and named A2-CL. According to different N/P ratios (N is the amount of nitrogen in A2-CL and P is the amount of phosphate in Dbait), varying concentration of A2-CL solution was added to Dbait in equivalent volume to form A2-CL/Dbait and let it stand for about 20 min at room temperature.

The mixture of PLGA-PEG-Mal [the abbreviation of Poly (lactide-co-glycolide)-b-poly (ethylene glycol)-maleimide] (Polyscitech, AI110; LA: GA = 50:50; M_W:: ≈30 000–5000 Da) and Angiopep-2 (GL Biomechem Ltd,180970) was added dropwise into the aqueous phase with the oil to water ratio of 3:7, which was then dialyzed in 3 L DEPC for 2 h as mentioned above to form A2-PLGA-PEG-Mal nanoparticles (A2-PLGA-PEG-Mal NPs). Then, A2-PLGA-PEG-Mal NPs were conjugated with anti-OX40 (BioXcell, clone: OX-86) at a mass ratio of 12:1 for 18 h at 4℃ through maleimide-thiol click chemistry [22, 25] .

The size (nm) of A2-CL, A2-CL/Dbait, A2-PLGA-PEG-Mal and A2-PLGA-PEG-Mal/anti-OX40 were tested by Malvern Zetasizer Nano-ZS Instruments, which was also utilized for testing the zeta potential (mV) of A2-CL and A2-CL/Dbait. The zeta potential (mV) Each experiment was repeated three times. All NPs were diluted into 0.5 μg/μl, morphology of which were observed by the transmission electron microscopy (TEM).

Stability test

Stability test was used to evaluate the stability of A2-CL/Dbait and A2-PLGA-PEG-Mal/anti-OX40 NPs in different condition. A2-CL/Dbait and A2-PLGA-PEG-Mal/anti-OX40 NPs were cultured with fresh medium containing 10% FBS for three days, the size (nm) of which was tested by Malvern Zetasizer Nano-ZS Instruments every day.

Agarose gel electrophoresis assay

Agarose gel electrophoresis assay was conducted to assess the capability of A2-CL to load Dbait. A2-CL complexing solution loaded Dbait at NH_2^+/PO_4^- ratio (N/P ratios, mol: mol) 1/1, 2/1, 4/1, 6/1, 8/1, 10/1 and 12/1 respectively were prepared as described above for agarose gel electrophoresis assay. 1 g agarose was completely dissolved in 50 ml 1×TAE electrophoresis buffer, which was followed by adding 5 μl nucleic acid gel stain (VICMED, VN302-500). After the agarose was completely solidified at room temperature, the freshly prepared samples were added for electrophoresis at the voltage of 120 V for 30 min. Agarose gel was visualized and photographed by the UV transilluminator (Tanon-1600).

Cell cytotoxicity and viability assays

CCK8 assay was used to evaluate cytotoxicity of A2-CL and A2-CL/Dbait NPs. G422, GL261 and LO_2 cells were seeded in 96-well plates at an appropriate cell density. After cell adhesion, the complete medium was replaced with fresh medium containing A2-CL and A2-CL/Dbait at a concentration of 1 μg/mL of Dbait. The changes in cell number were detected with a CCK-8 assay kit (Vicmed, VC5001L) continuously for 4 days according to manufacturer's instruction. Each experiment was repeated three times.

MTT as well as live and dead cell staining assay were used to assess the effect of A2-CL and A2-CL/Dbait NPs on GBM cells viability and proliferation. For MTT assay, following similar seeding and treatment procedures as described in the CCK8 assay and incubate the cells with the treatment medium (with PBS, A2-CL or A2-CL/Dbait NPs) for 24 h. Remove the treatment medium and wash the cells with PBS twice. Add 0.5% MTT solution (5 mg/ml) (KeyGEN BioTECH, KGA9301-1000) to each well and incubate the cells in 37℃, 5% CO_2 incubator for 4 h. Then, MTT solution were carefully replaced with 150 μl DMSO per well. Incubate them in the dark with gentle shaking at room temperature for 10 min. Optical density (OD) values at 495 nm were read, recorded, and analyzed.

For live and dead cell staining assay, LO_2 cells were seeded in 6-well plate and similar treatment procedures were followed as described in the MTT assay. After treatment and washing (as described above), stain the cells using the live/dead cell staining test kit according to the manufacturer's instructions (KeyGEN BioTECH, KGA9501-1000). 2μM Calcein AM and 8μM PI working solution were added to each well and incubate them in the dark at room temperature for 30 min. Cells were washed with PBS and photographed under a fluorescence microscope. Live cells were labeled with green fluorescence (Calcein AM, Ex/Em:495/520) and dead cells were labeled with red fluorescence (PI, Ex/Em:530/620).

Endosomal escape and transfection efficiency assay

Endosomal escape assay was used to observe the endocytosis and release of A2-CL/Cy-5-Dbait NPs [24, 26]. G422 and GL261 cells were seeded into 12-well plates containing sterile cover glass at appropriate cell densities. When the cell density reached approximately 60-70%,

the complete medium was replaced with serum-free medium containing A2-CL/Cy5-Dbait NPs at a concentration of 1 μg/mL of Dbait. According to the incubation time after NPs transfection, the experiment was divided into 4 groups: 3 h group, 4 h group, 5 h group and 6 h group. After respective incubation times (3 h, 4 h, 5 h and 6 h), fresh DMEM medium containing Lyso-Tracker Green (BeyoTime, C1048) solution was added to incubate at 37℃ for 20 min in the dark, which was replaced by Hoechst33324 for 20 min at room temperature in the dark. Cells adhered to sterile cover glass were fixed with 4% paraformaldehyde solution for 10 min. Laser confocal microscopy was used to observe the lysosome staining and Cy5-Dbait nucleation.

For transfection efficiency assay, follow the same NPs transfection protocol as described above, and perform nuclear staining with Hoechst33324 after 24 h of NPs transfection. The expression of red fluorescence in the cells was observed by fluorescence microscope, and the transfection efficiency was calculated following this formulation: transfection efficiency (%) = number of cells expressing red fluorescence/total number of cells×100%.

Colony formation assay

Colony formation assay was used to evaluate the radiation sensitivity effects of A2-CL/Cy5-Dbait NPs. G422 and GL261 cells were seeded into 6-well plates respectively at appropriate cell densities. After cell adhesion, GBM cells were transfected with A2-CL/Cy5-Dbait NPs or A2-CL NPs at a concentration of 2 μg Dbait/2mL/well of Dbait. 5–6 h after transfection, GBM cells were irradiated with 0 Gy, 2 Gy, 4 Gy, 6 Gy and 8 Gy at the dose rate of 300 cGy/min respectively. Approximately 10–14 days later, cell clones with over 50 cells, fixed with 4% paraformaldehyde and stained with crystal violet, were counted by Image J software. Dose-Survival fraction (SF) curve of GBM cells were fitted by GraphPad Prism 8.0 software as the following two formula: one is single-hit multitarget model: $SF = 1-(1-e^{-D/D0})^N$, $Dq = D0 \times \ln N$; one is linear–quadratic model: $SF = e^{-D(\alpha+\beta D)}$. Sensitization enhancement ratio (SER) was calculated as dividing D0 of control group by D0 of experimental group (SER_{D0}).

Western blot (WB) assay

WB assay was used to assess the effect of A2-CL/Cy5-Dbait NPs on DSBs. The adherent GBM cells were seeded in 6 cm plates at appropriate cell densities. A2-CL NPs or A2-CL/Cy5-Dbait NPs transfection was operated as colony formation assay and all GBM cells were irradiated with 6 Gy after 5 h transfection. According to the various time after irradiation (0 h, 2 h, 4 h, 6 h, 8 h and 24 h), cells were harvested for WB to test γ-H_2AX expression as previous study [7, 27]. For Phospho-P53 (Ser15) (p-P53) and DNA-PKcs expression, cells were harvested post 24 h irradiation or 24 h post NPs transfection. Primary antibodies, γ-H_2AX and p-P53 were obtained from Cell Signaling Technology (CST, #7631 and #9284 respectively) ; GAPDH and DNA-PKcs were obtainted from Proteintech (60004-1-Ig and 19983-1-AP respectively). Secondary antibodies were obtained from Vicmed (VA001 or VA002). Each WB was repeated three times and the band intensity was analyzed by Image J software.

Antigens capture in vitro

G422 and GL261 glioma cells were seeded into 10 cm plates. After cell densities up to 90-100%, the complete medium was replaced by serum-free medium and GBM cells were irradiated with 35 Gy at a dose rate of 500 cGy/min. 48 h after irradiation, the supernatant was collected, protein concentration of which was measured. The supernatant was incubated with diverse conjugation ratios of A2-PLGA-PEG-Mal/anti-OX40 NPs. 24 h and 48 h later, the particle size of NPs and the protein concentration of the supernatant were measured again.

GBM tumor inoculation in situ and treatment in vivo

All animal experiments were conformed to the guidelines of Jiangsu Council on Animal Care. KM mice (for G422 tumor inoculation) and C57BL/6 mice (for GL261 tumor inoculation), aged 4–6 weeks, were purchased from GemPharmatech company and housed at the SPF-level Laboratory Animal Center in Xuzhou Medical University. Mice were adaptively reared for one week before experiment. The mice were anesthetized and once anesthetized, mice were securely fixed in a brain stereotaxic frame for accurate position. 12×10^4 G422 cells in 2 μl PBS or 8×10^5 GL261 cells in 12 μl PBS were injected into the right striatum of mice by microinjection needle at the injection rate of 1 μl/min. For the retumorigenesis test, 15×10^5 GL261 cells were implanted in C57BL/6 mice. The needle was held in place for at least 5min post-injection to allow proper cell distribution and minimize backflow. The successful establishment of the GBM tumor model was confirmed by assessing luciferase fluorescence intensity using a small animal imaging system.

For NPs targeting and distribution in vivo, two weeks post GL261 cells injection, PBS, Free-Cy3-siRNA, A2-CL/Cy3-siRNA or A2-PLGA-PEG-Mal/AF647-anti-OX40 NPs were injected intravenously (AF647: Alexa Fluor™ 647 was purchased from ATT Bioquest®, catalog number:1278). 6 h and 24 h post NPs injection, NPs distribution in organs was assessed using a small animal imaging system to measure fluorescence intensity. 24 h after NPs injection, mice were sacrificed for slices of brain and other important organs, such as heart, liver, spleen, lung, and kidney. These organs were fixed in 4% paraformaldehyde, embedded in paraffin, and sectioned. Sections were stained with Hematoxylin & Eosin (H&E)

for histopathological analysis to evaluated NP-related tissue damage. Histopathological analysis was conducted by pathologist from the Affiliated Hospital of Xuzhou Medical University.

In the experiment of survival statistics, mice were intravenously administered A2-CL or A2-CL/Dbait NPs daily for three consecutive days with Dbait of 1 μg/g/day. 5–6 h after each daily NPs injection, mice received head radiation at a dose of 3 Gy. 24 h after the last radiotherapy session, mice were intravenously administered one of the following: A2-PLGA-PEG-Mal, free anti-OX40 antibodies or A2-PLGA-PEG-Mal/anti-OX40. Changes in GBM tumor bulk were observed using a small animal imaging system every week and evaluated with H&E staining at the same point. Sections used for H&E were collected 7 days (G422) and 10 days (GL261) after treatment. Mice were monitored for movement disorders or weight loss exceeding 50%, and the survival time of mice was recorded.

In CD8+T cells depletion assay, 350 μg anti-CD8 intraperitoneally 24 h before each treatment. All treatment were as the same mentioned before. Changes in GBM tumor bulk were observed using a small animal imaging system every week.

Immunofluorescence assay

G422 or GL261 tumor inoculation in situ and intravenous NPs injection were conducted as mentioned in the experiment of survival statistics. 10 days after A2-PLGA-PEG-Mal/anti-OX40 NPs injection, mice were sacrificed for the whole brain. The sections with the maximum tumor cross-sectional area was made into frozen sections, which were placed in citrate buffer solution (Vicmed, VIH105P) for antigen repair and blocked with 5% bovine serum albumin (BSA) solution for 1 h at room temperature, then incubated with the following primary antibody overnight at 4℃: CD4 (Abcam, ab183685), CD8 (Abcam, ab22378). After incubation with fluorescent secondary antibody (ABclonal, AS035; AS068) for 1 h, nuclear staining was performed with Hoest33324 for 20 min at room temperature free from light. The slides were sealed and photographed under a fluorescence microscope.

Cytokine detection and flow cytometry assay

G422 or GL261 tumor inoculation in situ and intravenous NPs injection were conducted as mentioned above. 10 days after A2-PLGA-PEG-Mal/anti-OX40 NPs injection, peripheral blood of mice was collected in tubes containing appropriate anticoagulant. The samples were centrifuged at 3000 g for 20 min at 4 ° C, which was repeated twice to obtain supernatant serum samples. The precipitate was used for flow cytometry assay. TNF-α, IFN-β, IL-10 and IL-12p70 cytokines in serum samples were detected using ELISA kit (BIO-RAD, 17007716) according to manufacturer's instruction by Luminex technology.

The precipitate obtained above was lysed in 6–8 times cell volume of Red Blood Cell Lysis Buffer (Beyotime, C3702-120 ml) for 10 min, centrifuged at 500 g for 3 min at 4℃ and the supernatant was discarded. FITC-CD4 (BD Biosciences, clone RM 4–5), APC-CD8a (BD Biosciences, clone 53−6.7) and PE-FoxP3 (BD Biosciences, clone R16-715) were diluted with 1×BD Perm/warm buffer (BD Pharmingen, 554714) to the concentration of 1 μg/ml. After incubation with 50 μl FITC-CD4 and APC-CD8a flow cytometry antibodies at 4℃ for 30 min, 150 μl BD CytoFix/ CytoPerm buffer (BD Pharmingen, 554714) was added and incubated at 4℃ for 20 min in the dark. Then samples were incubated with PE-FoxP3 overnight at 4℃ and resuspended in PBS for flow cytometry analysis. 1×10^5 immune cells were counted for incubation with flow cytometry antibodies and 1×10^4 immune cells were quantified by flow cytometry.

Statistical analysis

Quantitative data were presented as means±standard deviation (SD). T-test was used for comparing means between two groups and one-way ANOVA was used for comparing means among multiple groups. Kaplan-Meier (K-M) analysis was employed to estimate survival curves, and the Log-Rank test was applied to compare the survival curves among different groups. $P<0.05$ was considered statistically significant. Statistical analysis and graphical representations were performed by GraphPad Prism 8.0 software.

Results

A2-CL/Dbait nanoparticles Preparation and characterization

As shown in Fig. 2A-D, the size (nm) and zeta potential (mV) of A2-CL and A2-CL/Dbait NPs were measured by a Malvern ZetaSizer NanoZS. The diameter of A2-CL NPs increased from 42.843 nm to 81.137 nm and the zeta potential of A2-CL decreased from 43.800mV to 14.167mV upon interaction with Dbait (Fig. 2E). A2-CL/Dbait NPs were incubated in medium for three days, and the diameter changes were monitored daily. Results in Fig. 2B and **Supplementary Fig. 1** exhibited excellent stability of A2-CL/Dbait NPs over the incubation period. TEM images revealed that both A2-CL and A2-CL/Dbait NPs were spherical and uniformly dispersed, confirming the successful construction of the NPs (Fig. 2H). A gel retardation assay was conducted to determine the interaction efficiency between A2-CL NPs and Dbait. A2-CL NPs fully interacted with Dbait at an N/P ratio of 10:1 (Fig. 2F), which was chosen for subsequent experiments.

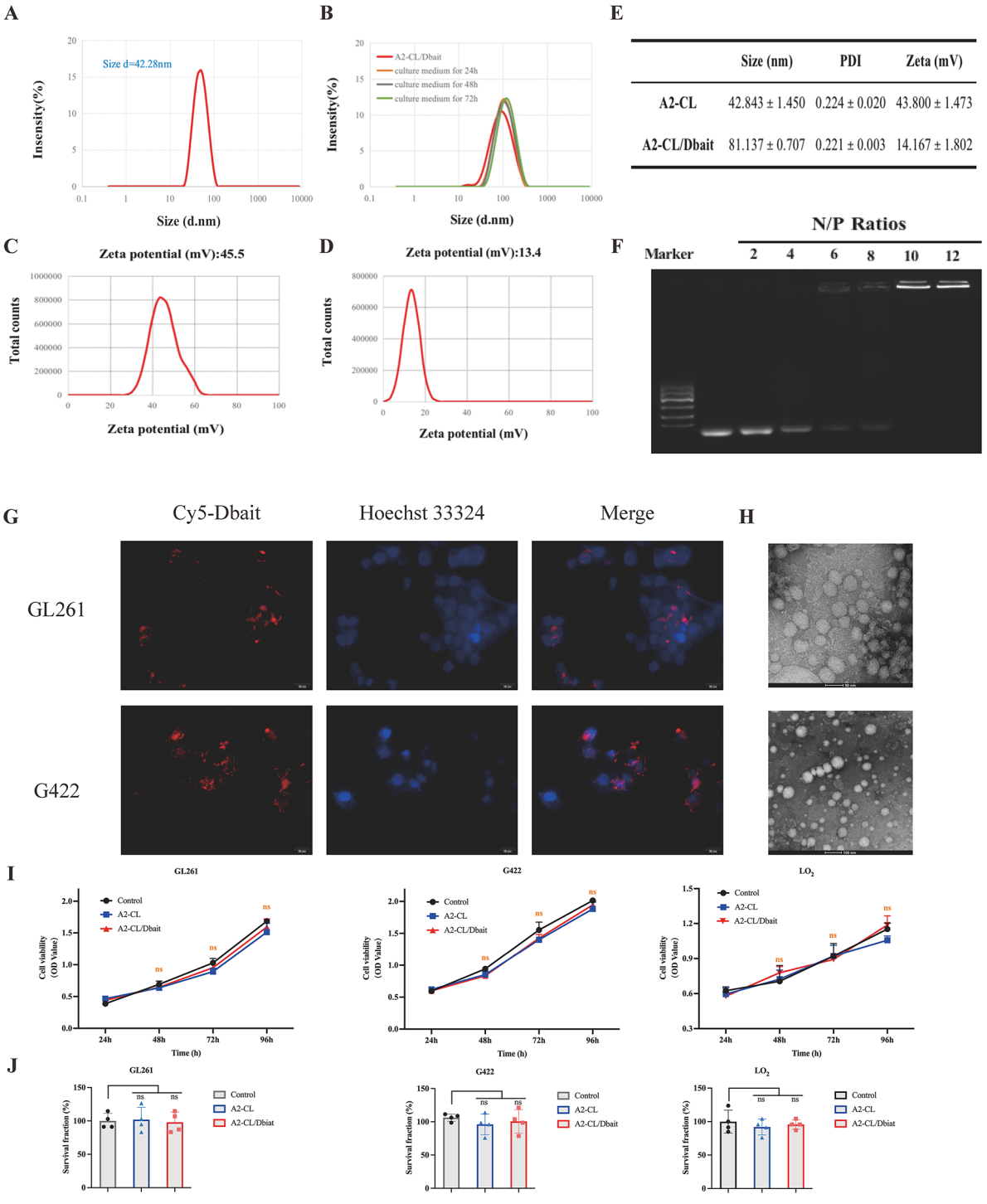

	Size (nm)	PDI	Zeta (mV)
A2-CL	42.843 ± 1.450	0.224 ± 0.020	43.800 ± 1.473
A2-CL/Dbait	81.137 ± 0.707	0.221 ± 0.003	14.167 ± 1.802

Fig. 2 Characteristics of A2-CL/Dbait NPs. (**A-B**) the diameter size (nm) of A2-CL NPs before (**A**) and after (**B**) interacting with Dbait by Malvern Zetasizer Nano-ZS Instruments; **(C-D)** zeta potential (mV) before (**C**) and after (**D**) interacting with Dbait by Malvern Zetasizer Nano-ZS Instruments; **(E)** the summary of basic parameters of A2-CL and A2-CL/Dbait NPs (¯x ± SD); **(F)** The encapsulation ability of A2-CL/Dbait NPs at different NH2+/PO4- ratio (N/P ratios, mol: mol) detected by agarose gel electrophoresis assay, N/P ratios = 1:10 indicated A2-CL NPs fully interacted with Dbait; **(G)** cell transfection efficiency of A2-CL/Cy5-Dbait NPs, which is 63.2% in GL261 and 90% in G422; (20 μm); A2-CL/Cy5-Dbait NPs were labeled by red fluorescence and cell nucleus was labeled by blue fluorescence; **(H)** the morphological structure of A2-CL/Dbait NPs detected by TEM; the top is A2-CL and the bottom is A2-CL/Dbait; **(I)** the effect of A2-CL/Dbait NPs on cell cytotoxicity by CCK8 assay, OD value were detected continuously for 4 days; **(J)** the effect of A2-CL/Dbait NPs on cells viability by MTT assays. ns: no significance

Low cytotoxicity and high cellular uptake efficiency of A2-CL/Dbait NPs

Low toxicity should be the essential condition for NPs delivering Dbait in vitro and in vivo. As shown in Fig. 2I, cell proliferation ability was not significantly affected following transfection with A2-CL and A2-CL/Dbait NPs, indicating that the NPs are low in toxicity, indicating minimal toxicity. MTT assays were performed to quantify cell viability and no significant reduction in cell viability was observed post-transfention with A2-CL and A2-CL/Dbait NPs, reinforcing the low toxicity of the NPs (Fig. 2J). Meanwhile, live and dead cell staining assay were conducted to further confirm NP toxicity. The ratio of green fluorescence (live) to red fluorescence (dead) remained similar across NP-treated and control groups, supporting the conclusion of low toxicity (**Supplementary Fig. 2**).

To investigate the transfection efficiency of A2-CL/Dbait NPs in GBM cells, A2-CL NPs were coated with Cy5-labeled Dbait to enable tracking of the transfected material. 24 h post-transfection of A2-CL/Cy5-Dbait NPs, G422 and GL261 cells were examined using an inverted fluorescence microscope. As shown in Fig. 2G, over 60% of GL261 cells and more than 90% of G422 cells exhibited red fluorescence.

Next, the endocytosis and release of A2-CL/Dbaits were observed by endosomal escape assay. As shown in Fig. 3 and h after transfection, red fluorescent A2-CL/Cy5-Dbait NPs were primarily localized within green fluorescent endosomes. 4–6 h post-transfection, a gradual release of Cy5-Dbait into the blue-stained nucleus was noted to exert its biological functions.

A2-CL/Dbait NPs exhibited satisfactory radiosensitization in vitro

The radiosensitization effect of A2-CL/Dbait NPs on GBM cell lines, G422 and GL261, was detected by clonal formation assay. Dose-survival curves fitting by single-hit multitarget model and linear-quadratic model revealed that the survival curves for the RT + A2-CL/Dbait groups exhibited a steeper decline with increasing irradiation dose compared to the RT and RT + A2-CL groups, which showed more gradual declines (Fig. 4A-D). SER_{D0} for A2-CL/Dbait was 1.637 for G422 cells and 1.678 for GL261 cells, indicating effective radiosensitization.

Since irradiation causes cell death by inducing DNA DSBs, γ-H_2AX was used as the indicator of DSBs. To measure the induction of DNA DSBs following irradiation with and without A2-CL/Dbait NPs, cells were irradiated and then harvested at various time points (0 h, 2 h, 4 h, 6 h, 8 h and 24 h) post-irradiation. In the RT and RT + A2-CL groups, γ-H_2AX levels rose significantly immediately after irradiation but returned to near-normal levels by approximately 8 h. In contrast, the RT + A2-CL/Dbait group showed a more substantial and prolonged increase in γ-H_2AX expression, which remained elevated up to 24 h post-irradiation, indicating persistent DNA damage (Fig. 4E-F).

To evaluate the effect of A2-CL/Dbait on DNA damage associated proteins expression, cells were irradiated and harvested 24 h post irradiation. Compared to the control and A2-CL group, DNA-PKcs and p-P53 expression levels in A2-CL/Dbait rose significantly, indicating the exist of Dbait effectively recruited DSB repair proteins. Similarly, compared to RT and RT + A2-CL group, DNA-PKcs and p-P53 expression levels in RT + A2-CL/Dbait increased significantly, reaffirming the ability of Dbait to recruit DSB repair proteins, thereby intensifying the DNA damage response post-irradiation (Fig. 4G-H).

Characterization and antigen capture of A2-PLGA-PEG-Mal/anti-OX40 NPs in vitro

The diameter of A2-PLGA-PEG-Mal NPs increased from 101.883 nm to 121.167 nm after conjugating anti-OX40 (Fig. 5A-C). TEM images confirmed the spherical structure of the NPs, validating successful A2-PLGA-PEG-Mal/anti-OX40 NPs construction (Fig. 5D). And A2-PLGA-PEG-Mal/anti-OX40 NPs cultured with medium also displayed fantastic stability, as evidenced by consistent results over time (Fig. 5B, **Supplementary Fig. 1**).

A2-PLGA-PEG-Mal and anti-OX40, conjugated with different ratios of 6:1, 12:1, 18:1, 24:1 and 30:1, were incubated with the supernatant collected from irradiated GBM cells. The concentration of antigen in the supernatant considerably decreased after captured by A2-PLGA-PEG-Mal/anti-OX40 NPs (Fig. 5E). The diameters of A2-PLGA-PEG-Mal/anti-OX40 NPs increased more than two-fold (Fig. 5F) after antigen capture. All of results collectively proved the excellent antigen capture capability of A2-PLGA-PEG-Mal/anti-OX40 NPs in vitro.

Favorable targeting and low toxicity of A2-CL/Dbait and A2-PLGA-PEG-Mal/anti-OX40 NPs in vivo

6 h and 24 h after PBS, free-Cy3-siRNA, A2-CL/Cy3-siRNA or A2-PLGA-PEG-Mal/AF647-anti-OX40 NPs injection intravenously, the fluorescence distribution in brain and other major tissues and organs of mice was observed by a small animal imaging system. Results in Fig. 6A-B, D revealed that free-Cy3-siRNA showed no distribution in brain and minimal distribution in liver and kidneys. However, A2-CL/Cy3-siRNA and A2-PLGA-PEG-Mal/AF647-anti-OX40 NPs abundantly distributed in brain with minimal distribution in other tissues and organs. Bulk red fluorescence from labeled NPs in GBM areas labeled by GFP, suggesting favorable targeting of both A2-CL/Dbait and A2-PLGA-PEG-Mal/anti-OX40 NPs (Fig. 6C, **Supplementary Fig. 3**).

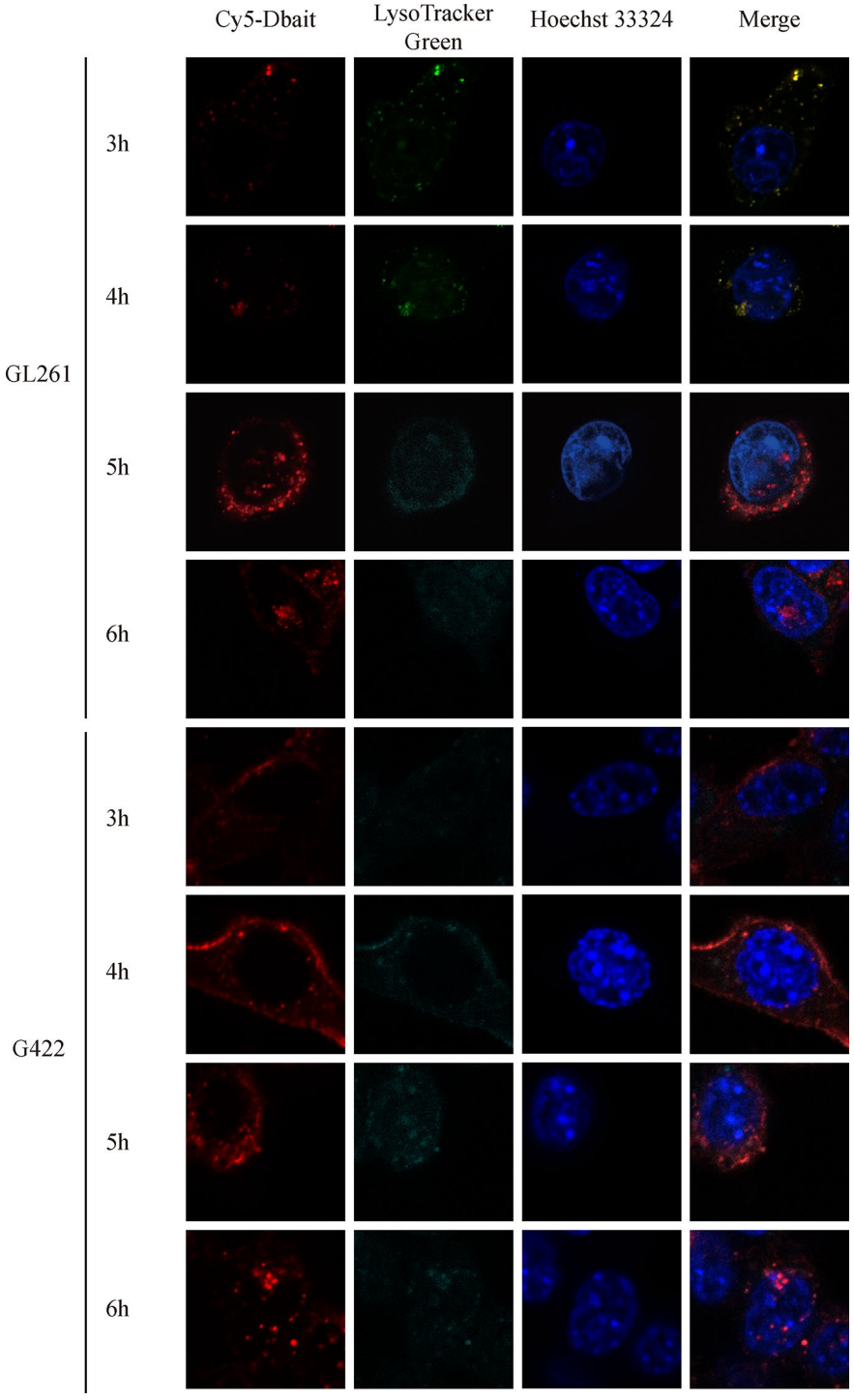

Fig. 3 The endocytosis and release of A2-CL/Cy5-Dbait by endosomal escape assay. (×1000). A2-CL/Cy5-Dbait NPs were labeled by red fluorescence, lyso tracker was labeled by green fluorescence, and cell nucleus was labeled by blue fluorescence

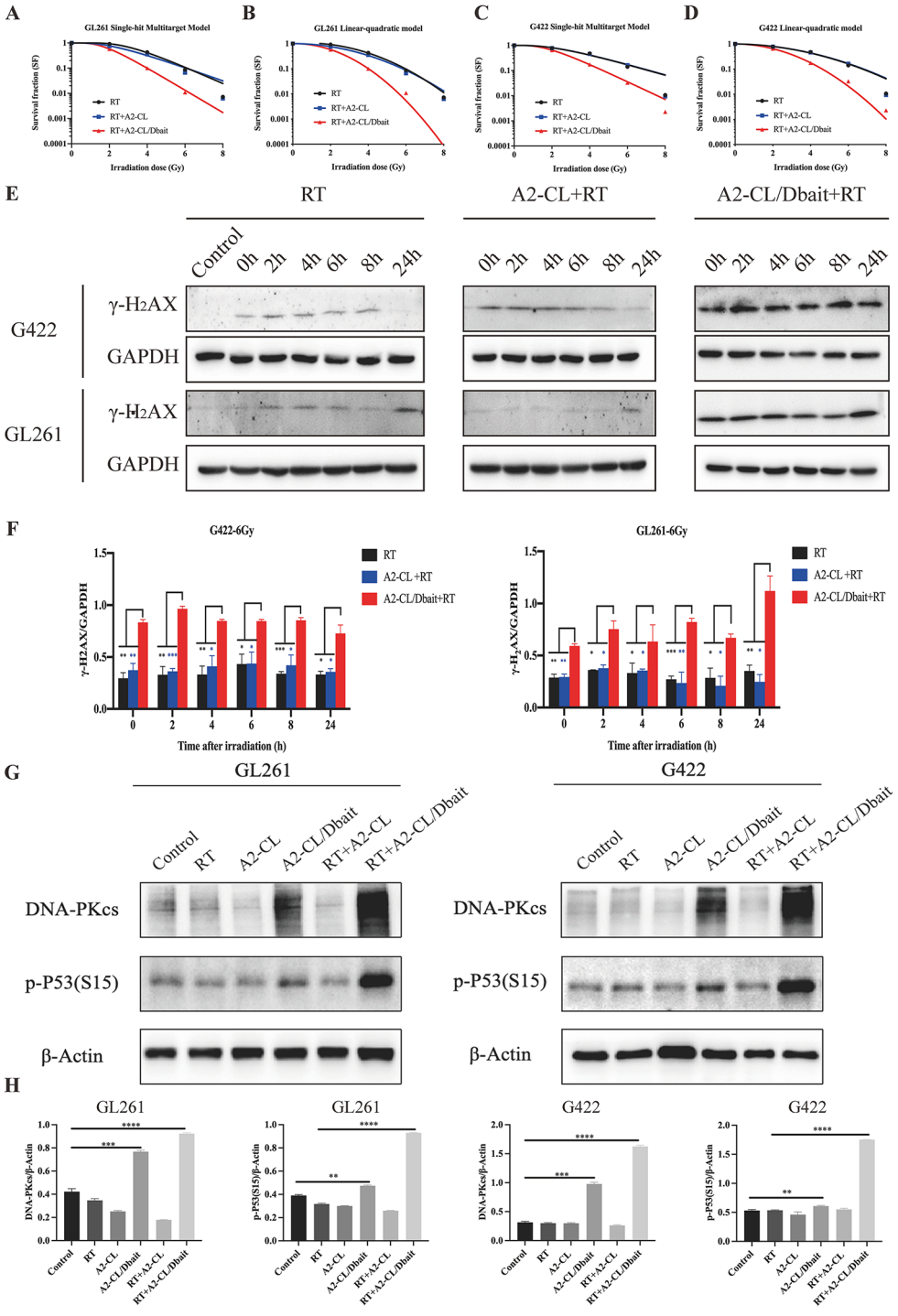

Fig. 4 Radiation sensitization effect of A2-CL/Dbait NPs on GL261 and G422 cells. (**A-D**) Dose-cell survival curves fitting by single-hit multitarget and Linear-quadratic models in GL261 (**A**-**B**) and G422 (**C**-**D**) cells; **(E-F)** γ-H_2AX expression at different time points after irradiation (**E**) and semi-quantitative statistical analysis of WB intensities (**F**); **(G-H)** DNA-PKcs and p-P53 (Ser15) expression after 24 h irradiation (**G**) and semi-quantitative statistical analysis of WB intensities (**H**). *$p < 0.05$, **$p < 0.01$,***$p < 0.001$,****$p < 0.0001$

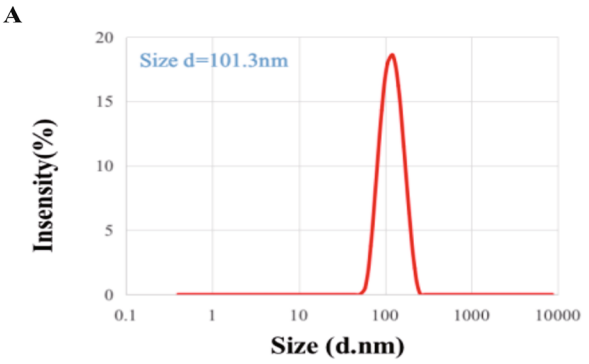

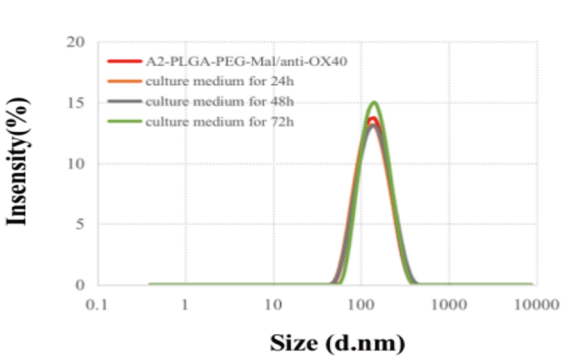

C

	Size (nm)	PDI
A2-PLGA-PEG-Mal	101.883 ± 2.282	0.066 ± 0.018
A2-PLGA-PEG-Mal/anti-OX40	121.167 ± 1.582	0.157 ± 0.002

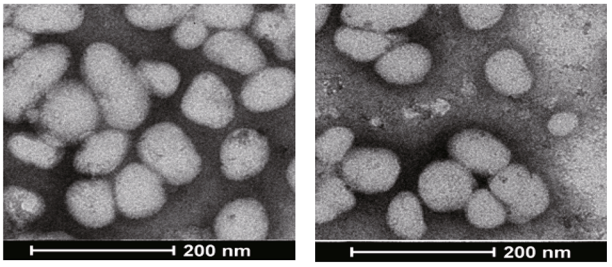

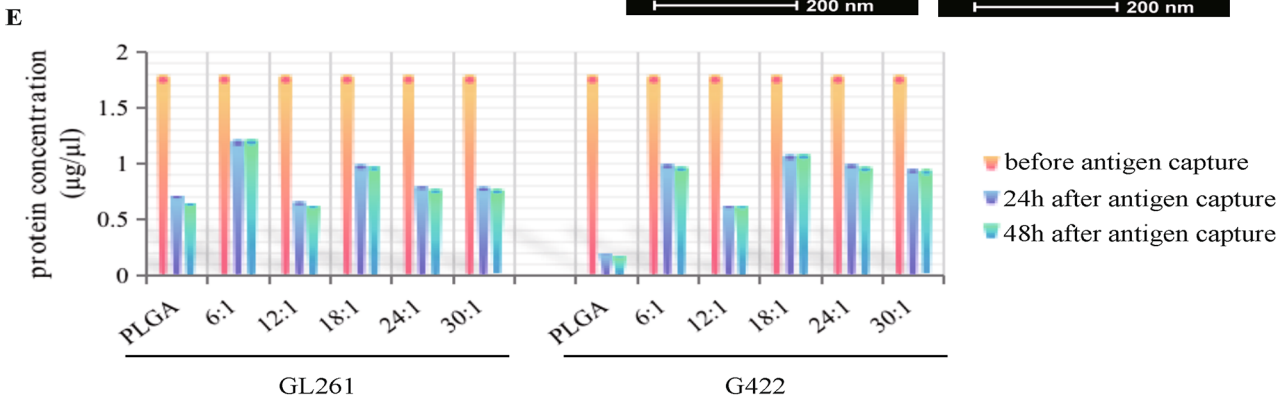

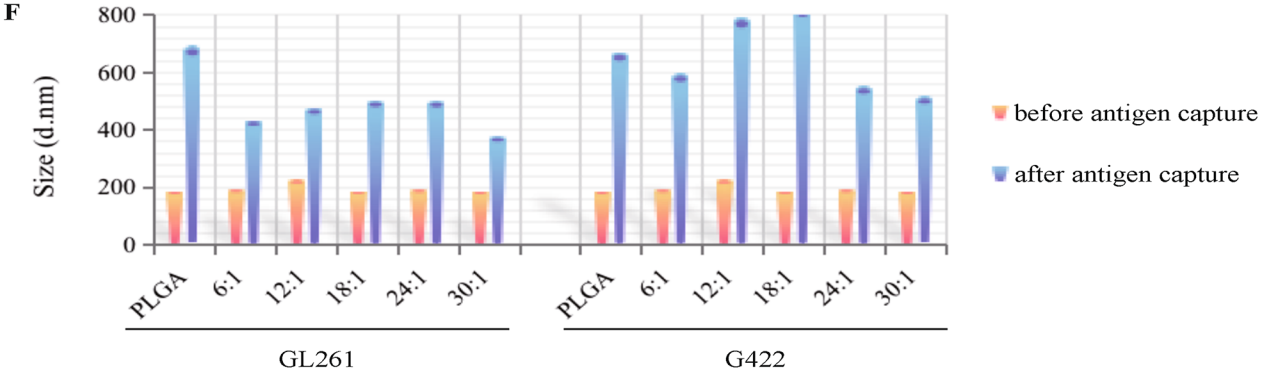

Fig. 5 Characteristics of A2-PLGA-PEG-Mal/anti-OX40 NPs. (**A-B**) the diameters (nm) of A2-PLGA-PEG-Mal/anti-OX40 NPs before (**A**) and after (**B**) conjugated with OX40 antibody by Malvern Zetasizer Nano-ZS Instruments; **(C)** basic parameters of A2-PLGA-PEG-Mal and A2-PLGA-PEG-Mal/anti-OX40 NPs by Malvern Zetasizer Nano-ZS Instruments (mean ± SD); **(D)** the morphological structure of A2-PLGA-PEG-Mal/anti-OX40 NPs detected by TEM; the left is A2-PLGA-PEG-Mal NPs and the right is A2-PLGA-PEG-Mal/anti-OX40 NPs; **(E)** the protein concentration of antigen supernatant before and 24 h, 48 h after incubating with A2-PLGA-PEG-Mal/anti-OX40 NPs with different conjugation mass ratios; **(F)** the size changes of A2-PLGA-PEG-Mal/anti-OX40 NPs with different conjugation mass ratios before and 24 h after antigen capture by Malvern Zetasizer Nano-ZS Instruments

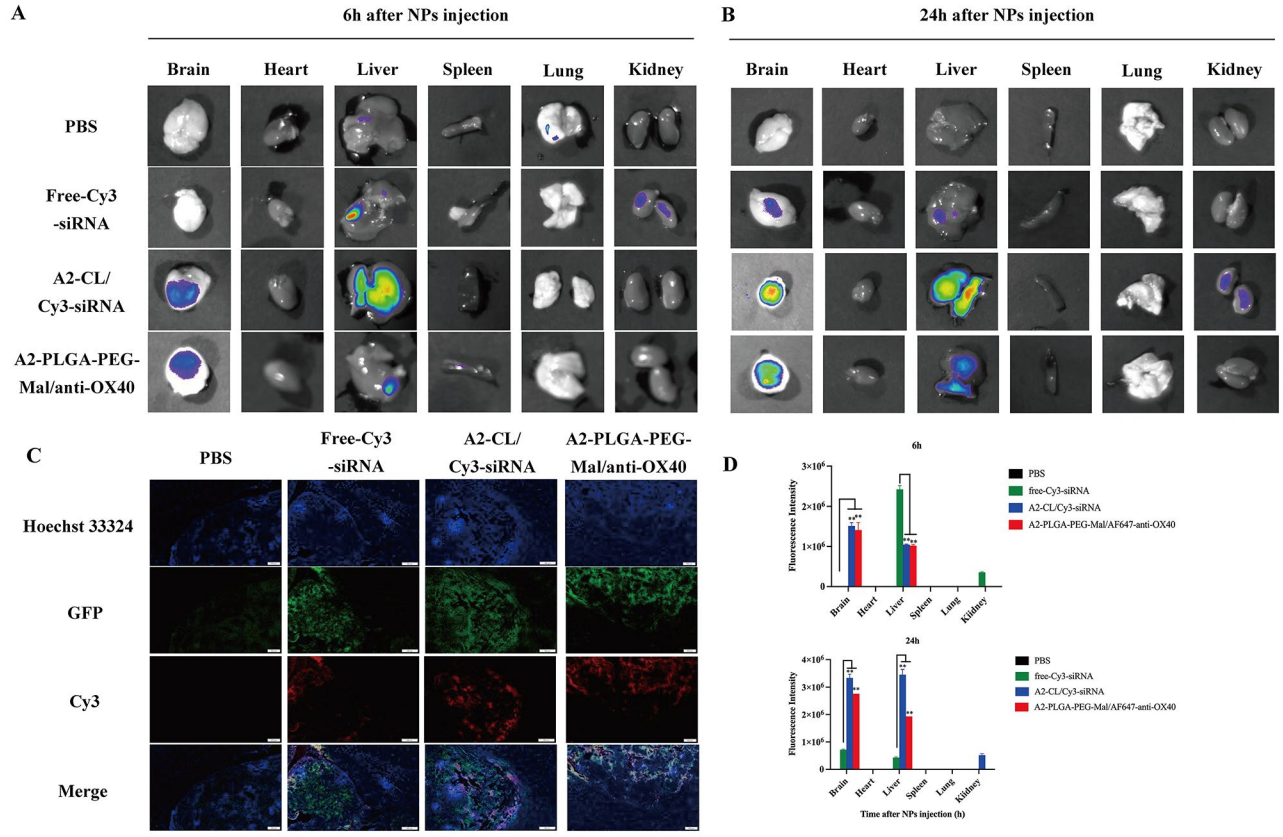

Fig. 6 The targeting and distribution of A2-CL/Dbait and A2-PLGA-PEG-Mal/anti-OX40 NPs in vivo. (**A-B**) the distribution of A2-CL/Cy3-siRNA and A2-PLGA-PEG-Mal /AF647-antiOX40 NPs 6 h **(A)** or 24 h **(B)** after intravenous injection by a small animal imaging system; **(C)** the distribution of NPs post 24 h injection via tail vein in GL261 glioma-bearing mice observed by immunofluorescence (100 μm), A2-CL/Cy3-siRNA or A2-PLGA-PEG-Mal /AF647-antiOX40 NPs were labeled by red fluorescence, GL261 GBM tumor area was labeled by green fluorescence, cell nucleus was labeled by blue fluorescence; **(D)** fluorescence intensity in different organs (brain, heart, liver, spleen, lung and kidney) 6 h and 24 h post injection of indicated NPs. $^{**}p < 0.01$

Next, we investigated the potential damage caused by A2-CL/Dbait and A2-PLGA-PEG-Mal/anti-OX40 treatment on major tissues and organs. Images stained by H&E in Fig. 7**and Supplementary Fig. 4** showed no noticeable histopathological damage for all groups of mice, suggesting both A2-CL/Dbait and A2-PLGA-PEG-Mal/anti-OX40 NPs were well tolerated in vivo.

The combination of A2-CL/Dbait and A2-PLGA-PEG-Mal/anti-OX40 NPs prolonged survival time in vivo

The treatment regimen for mice was performed as shown in Fig. 8A. The statistical results of overall survival (OS) were listed in Fig. 8B, showing that neither local radiotherapy for head nor cationic liposome (A2-CL) combined with local radiotherapy significantly prolonged the median survival time (RT vs. A2-CL+RT vs. control: 24 days vs. 24 days vs. 24 days for GL261 cells; 16 days vs. 13 days vs. 13 days for G422 cells), while RT combined with A2-CL/Dbait injection significantly prolonged the OS (median survival time: RT+A2-CL/Dbait vs. RT+A2-CL: 35 days vs. 24 days for GL261cells; 16 days vs. 13 days for G422 cells). Further combining A2-CL/Dbait with local RT and A2-PLGA-PEG-Mal/anti-OX40 resulted in extended OS and achieved 40—60% complete remission (CR) in vivo. Head fluorescence imaging (Fig. 8D) and H&E staining (Fig. 9) provided visual confirmation of treatment effectiveness with reduced tumor burden and enhanced therapeutic outcomes. Not only that, it is excellent that mice achieving CR showed resistance against re-implantation of GL261 cells three months later, demonstrating successful tumor eradication (Fig. 8C). Moreover, considering that simple delivery of free anti-OX40 antibody may sometimes cross and disrupt BBB in orthotopically implanted models, the effect of combination of A2-CL/Dbait and free anti-OX40 antibodies was also evaluated. As shown in Figs. 8B and D and 9, the simple delivery of anti-OX40 did not inhibit tumor growth or extend OS comparing with A2-CL/Dbait+RT, highlighting the significant improvements in survival and therapeutic outcomes achieved through the innovative combination of RT, A2-CL/Dbait and A2-PLGA-PEG-Mal/anti-OX40 NPs in treating GBM in mouse models.

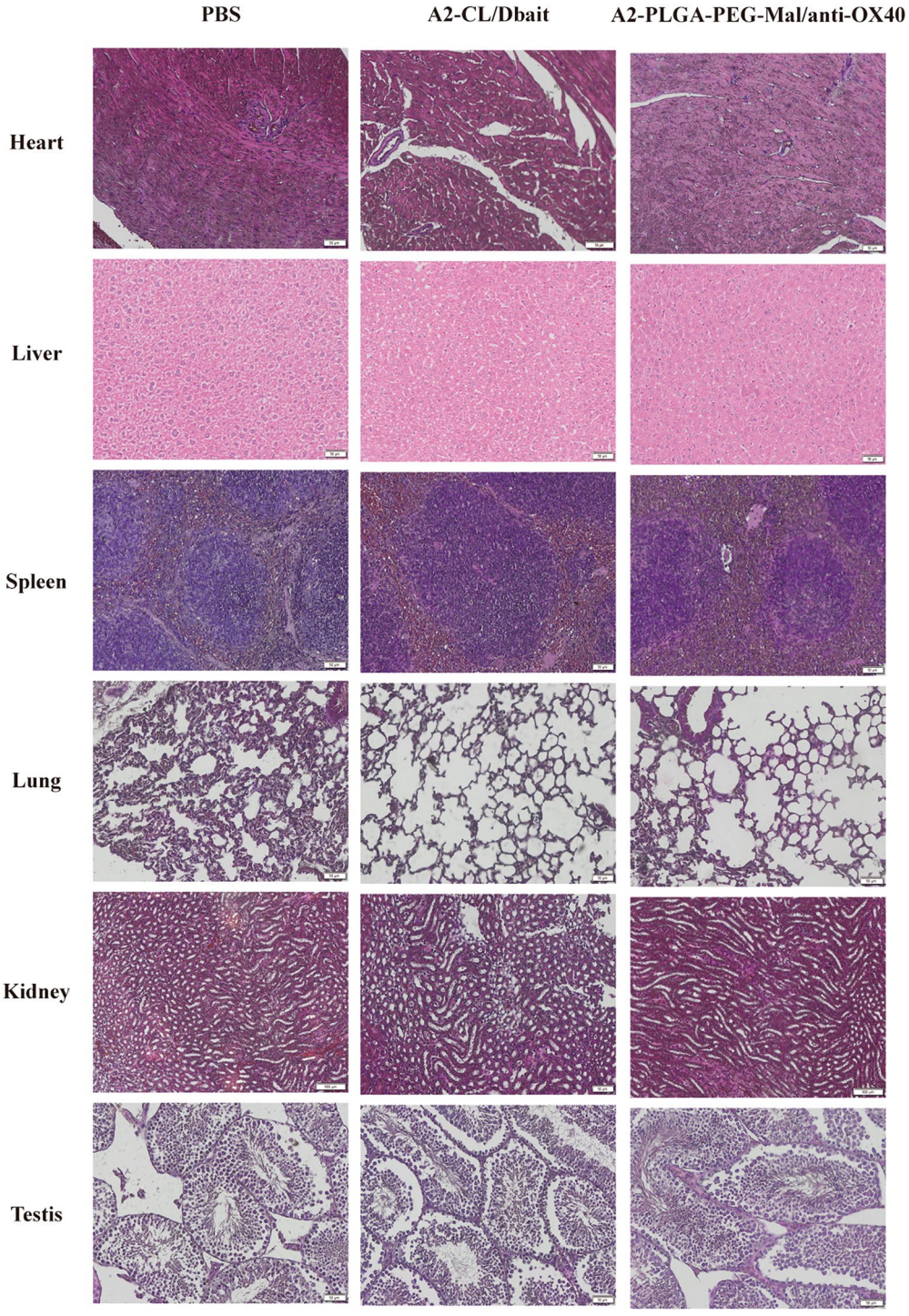

Fig. 7 The toxicity of A2-CL/Dbait and A2-PLGA-PEG-Mal/anti-OX40 NPs on major tissues and organs by H&E (50 μm). The major tissues and organs including heart, liver, spleen, lung, kidney, and testis. Histopathological analysis was conducted by pathologist from the Affiliated Hospital of Xuzhou Medical University

The treatment of various NPs promoted CD8 + T cells infiltration and cytokine secretion

Cytokines including TNF-α, IFN-γ, IL-10 and IL-12p70 in mouse sera were tested by luminex technology at 10 days after A2-PLGA-PEG-Mal/anti-OX40 treatment. As shown in Fig. 10A-B, local radiotherapy, application of A2-CL/Dbait as well as A2-PLGA-PEG-Mal/anti-OX40 NPs promoted cytokine secretion, which multiplied in group of RT + A2-CL/Dbait + A2-PLGA-PEG-Mal/anti-OX40 NPs compared with group of RT + A2-CL/Dbait.

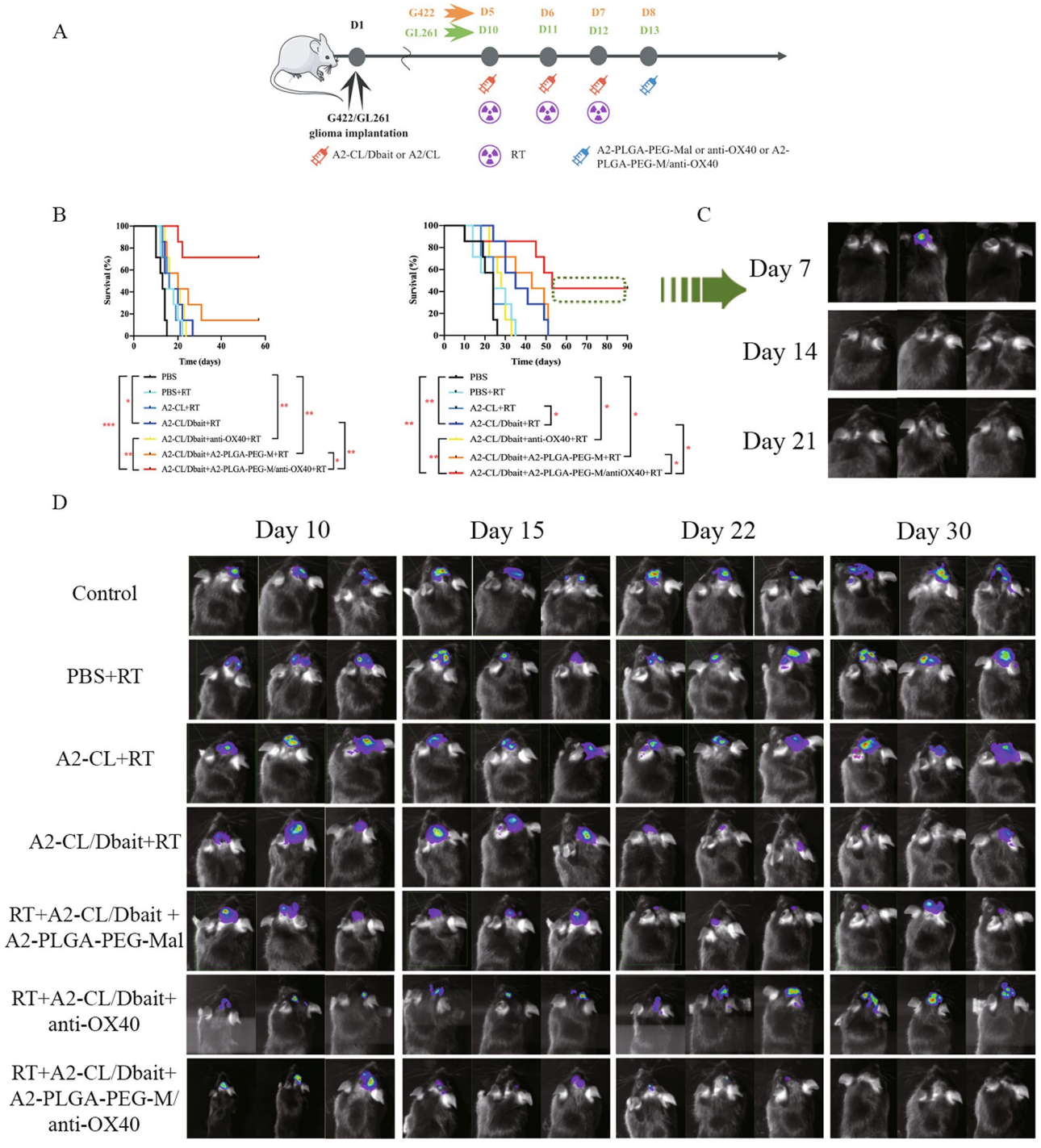

Fig. 8 The effect of combination of A2-CL/Dbait and A2-PLGA-PEG-Mal/anti-OX40 NPs on overall survival and tumor control of G422 and GL261 glioma-bearing mice in vivo. (**A**) Schematic diagram depicting experimental design and timeline of mouse model with different treatment; **(B)** Survival curves of KM and C57BL/6 mice implanted with G422 and GL261 cells respectively, $*p < 0.05$, $**p < 0.01$, $***p < 0.001$; (**C**) In retumorigenesis experiment, 7, 14 and 21 days after GL261 reimplanted in C57BL/6 mice experienced complete response, head fluorescence imaging were detected by a small animal imaging system; (**D**) head fluorescence imaging of in situ GL261 glioma bearing mice treated with indicated NPs were detected by a small animal imaging system at different time points (Day 10, Day 15, Day 22 and Day 30)

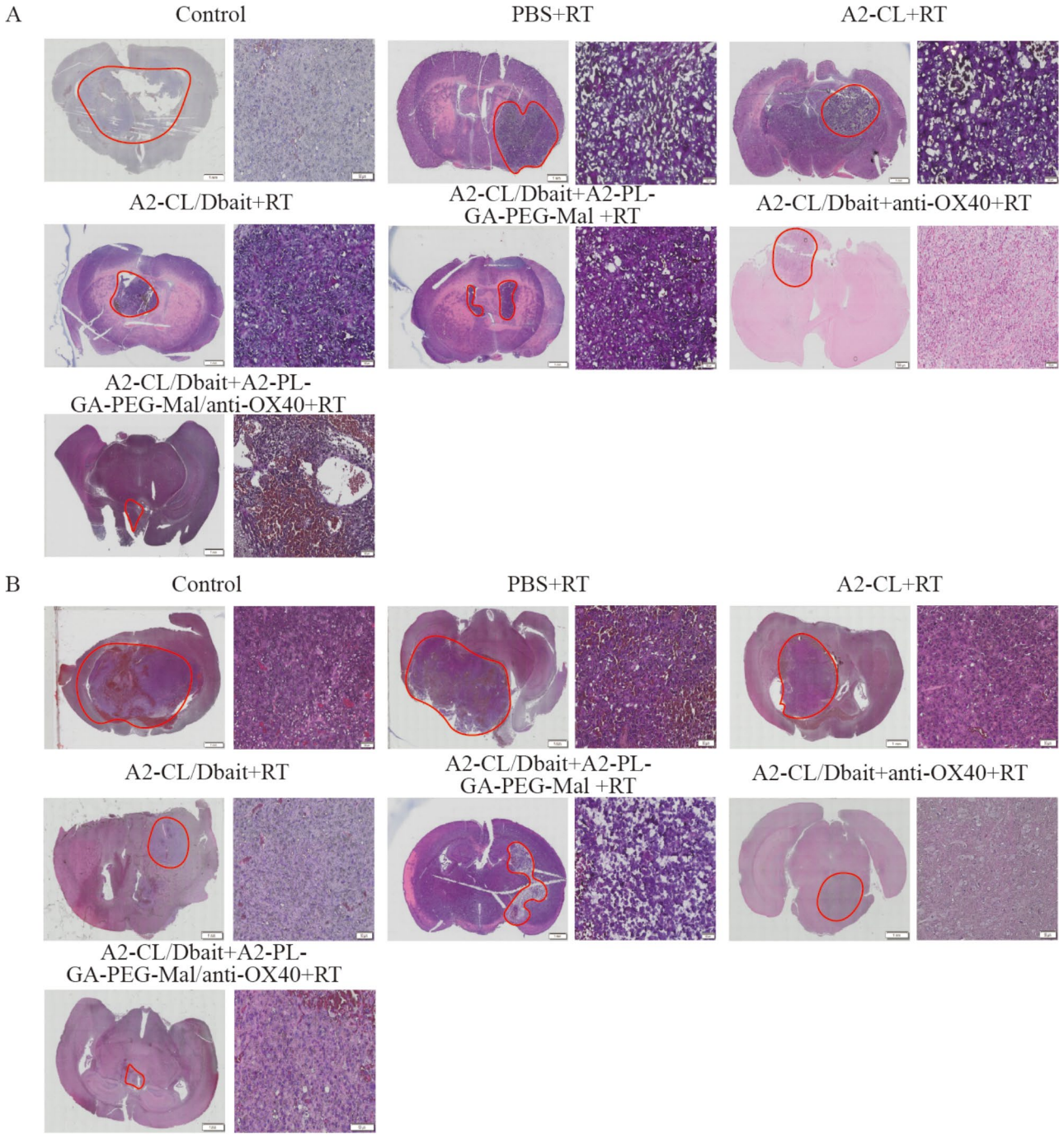

Fig. 9 The effect of A2-CL/Dbait combining with A2-PLGA-PEG-Mal/anti-OX40 on GL261 GBM (**A**) and G422 GBM (**B**) bulk control by H&E. GBM regions were highlighted with red circles. GL261 sections and G422 sections were collected 10 days and 7 days after treatment respectively. Images on the left is 1 mm and the right is 50 μm in each groups

Next, percentages of CD8+T cells and Treg cells were analyzed by flow cytometry (Fig. 10C-E). A2-PLGA-PEG-Mal/anti-OX40 NPs stimulated CD8+T cells differentiation and suppressed Treg cells, which synergistically excited antitumor immune response. Not only that, CD4+and CD8+T cells infiltration in glioma in situ were stained by immunofluorescence (Fig. 11**and Supplementary Fig. 5**). Evidently, the fluorescence intensity of CD4 and CD8 in the glioma site was significantly stronger in the group of A2-CL/Dbait+A2-PLGA-PEG-Mal/anti-OX40+RT than their counterparts in other groups, suggesting that A2-PLGA-PEG-Mal/anti-OX40 NPs could

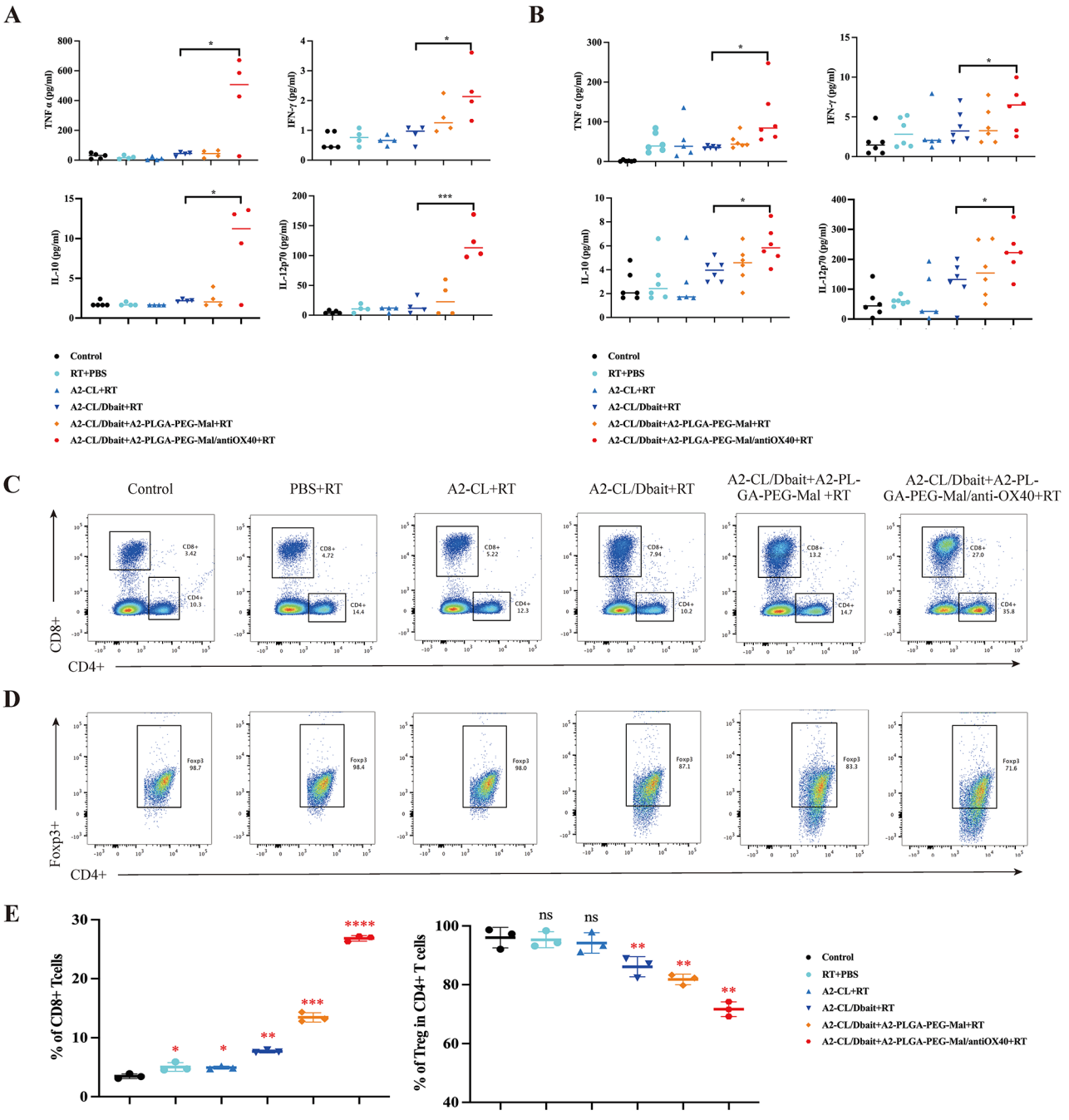

Fig. 10 The effect of A2-CL/Dbait and A2-PLGA-PEG-Mal/anti-OX40 NPs on antitumor immune response in peripheral blood from tumor-bearing mice. (**A**-**B**) cytokine secretion (TNF-α, IFN-γ, IL-10, IL-12p70) in sera from G422 (**A**) and GL261 (**B**) glioma-bearing mice at 10 days post the injection of indicated NPs by ELISA; **(C-D)** percentages of CD8+T cells (**C**) and Treg cells (**D**) at 10 days post the injection of indicated NPs from GL261 by flow cytometry; **(E)** statistical results of flow cytometry. ns: no significance, *$p < 0.05$, **$p < 0.01$, ***$p < 0.001$, ****$p < 0.0001$

significantly promote the invasion of tumor-associated lymphocytes.

To validate the dependency of anti-OX40 effect on T cells, we conducted a CD8+T cell depletion assay. The results, illustrated in **Supplementary Fig. 6**, showed that the substantial reduction in tumor size achieved with the combined treatment regimen was nullified upon CD8+T cell depletion. This demonstrated that the significance therapeutic benefit observed with the combination of A2-CL/Dbait, A2-PLGA-PEG-Mal/anti-OX40 and RT was lost following the depletion of CD8+T cells, which are crucial for mediating the observed anti-tumor response.

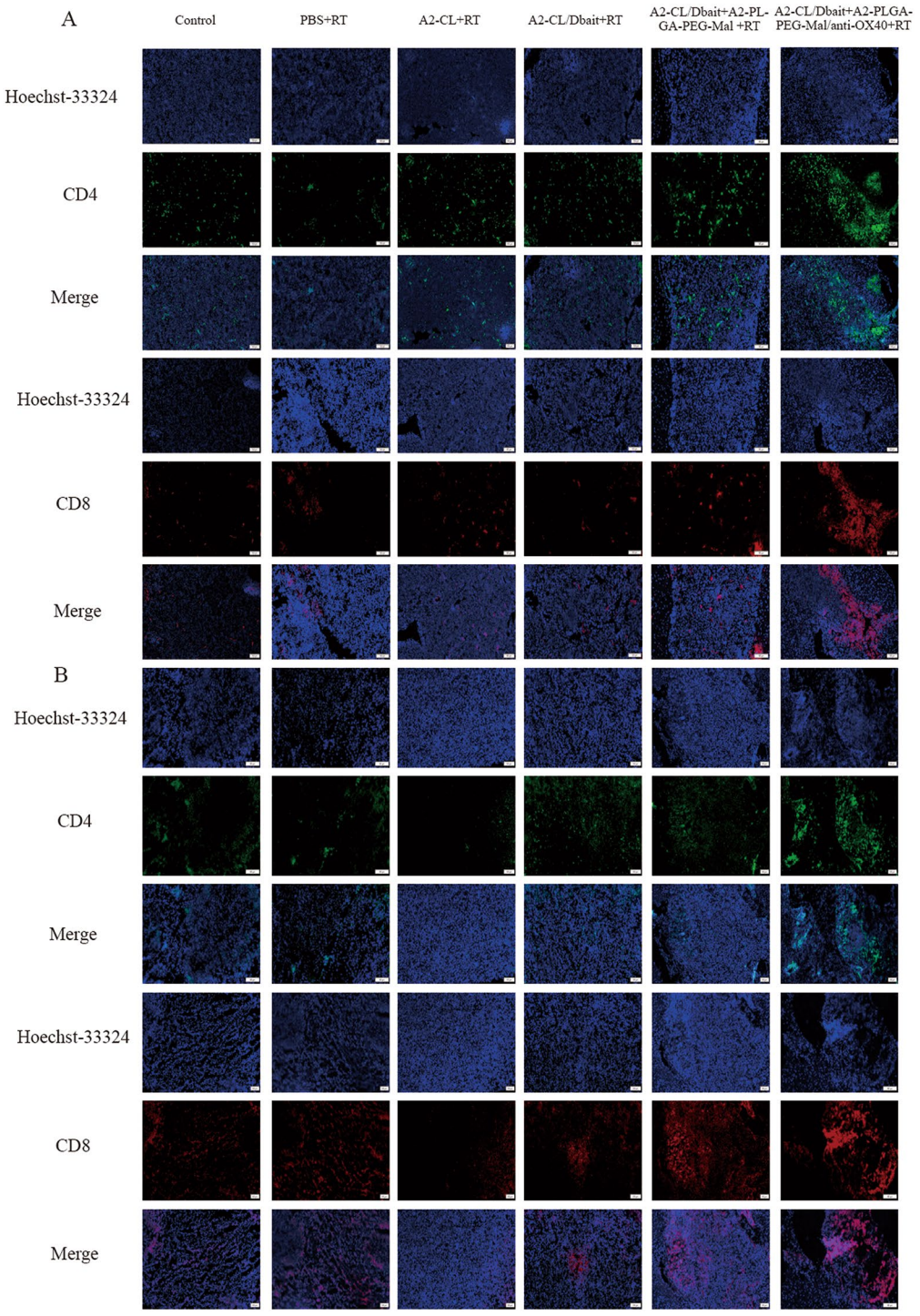

Fig. 11 Analysis of CD4 + T cells and CD8 + T cells infiltration in GBM bulk 10 days after different indicated NPs injection and treatment by immunofluorescence assay. (**A**) is for GL261 glioma bearing mice and **(B)** is for G422 glioma-bearing mice (100 μm). CD4 + T cells were labeled by green fluorescence, CD8 + T cells were labeled by red fluorescence and cell nucleus were labeled by blue fluorescence

Discussion

GBM, the most common primary brain malignancy in adults, is characterized by high malignancy, significant local invasiveness, and a high recurrence rate post-surgery, resulting in exceedingly poor treatment outcomes and progmosis [28, 29]. Despite the application of various advanced diagnosis and treatment technologies over the past decades, the median survival time for GBM patients remains less than 15 months [30]. Addressing challenges such as radiation resistance, BBB and "immune

immunity" of the CNS are critical areas of research aimed at improving the OS of GBM patients.

A "STUPP" protocol, widely recommended by NCCN guidelines for newly diagnosed GBM, represents the standard treatment regimen [31]. Despite its widespread use, the 5-year survival rate remains around 10%, highlighting the high tolerance of GBM cells to chemoradiotherapy. Over the years, radiobiologists have explored various approaches to enhance radiosensitivity targeting tumors at levels from cell to organs to the whole organism, from traditional hypoxic cell sensitizers to more complex strategies [32]. Almost involving tumor microenvironment (such as IL-2 combination with SBRT) [33], cell angiogenic factors [34] (vascular endothelial growth factor or epidermal growth receptor inhibitors), DNA damage repair (such as mirin, ATM/ATR inhibitors, DNA-PKcs inhibitors, etc.) [32], cell cycle regulation (such as Chk1/Chk2 inhibitors, CDK4/6 inhibitors) [32] and other aspects. Nearly 100 types of radiosensitizers have been studied, however, despite extensive research, few of which have advanced to clinical application due to issues such as intolerant side effects, single target actions, secondary resistance and limited efficacy.

Different from other radiosensitizers against a single target such as PARP inhibitors, ATM inhibitors, Dbait, initially reported by Marie Dutrex in 2009, is an ideal radiosensitizer simultaneously interfering with multiple pathways and multiple targets with low toxicity [6, 35]. In preclinical study, Dbait was proved excellent radiosensitizer in colorectal cancer [36], melanoma [5], prostate cancer [24], esophageal cancer [37] and glioma [38, 39]. The I/IIa clinical trial from 2015 to 2016, 5' cholesterol modified Dbait (DT01) (NCT01469455) was carried out in France [40], which enrolled 27 patients with metastatic melanoma. The results showed the safety and tolerability of DT01 at dose of 16 and 32 mg, with an encouraging overall response rate of 68% and a CR rate of 30%. In our study, the low toxicity and excellent radiosensitizer of Dbait was confirmed both in vitro and in vivo. However, Dbait, a small molecule DNA, is susceptible to degradation by DNase in vivo. In NPs targeting assay, free Cy5-siRNA were mainly distributed in liver and kidney with no distribution in brain and GBM. To address this, A2-modified cationic liposomes, known for their ability to target the BBB and deliver payloads to the GBM nucleus, were selected as the preferred carrier material for encapsulating Dbait in our study [41, 42].

Cationic liposomes consist of lipid bilayers with a combination of neutral phospholipids and positively charged cationic lipids. This combination is similar to biological membranes, allowing for effective electrostatic interactions with negatively charged Dbait, thereby facilitating cellular uptake [43, 44]. In our study, Cationic liposomes demonstrated a 90% transfection efficiency in G422 glioma cells, which was slightly lower in GL261 cells. Despite this, the SER_{D0} values exceeding 1.6 in colony formation assay confirmed the ideal radiosensitization effect provided by A2-CL/Dbait in both glioma cell lines. Notably, the survival curve for RT + A2-CL group made no significant change compared to RT group, indicating that A2-CL alone did not affect GBM cell radiosensitivity. It is the Dbait released from A2-CL/Dbait that contributes to the observed radiosensitization effect.

To further explore the mechanism of radiation sensitization by A2-CL/Dbait, we assessed the expression levels of γ-H_2AX, DNA-PKcs and p-P53(Ser15) by WB assay. Compared to RT and RT + A2-CL groups, the combination of RT and A2-CL/Dbait treatment significantly increased γ-H_2AX, DNA-PKcs and p-P53 (Ser15) expression. γ-H_2AX is a marker closely associated with DNA DSBs and the higher γ-H_2AX expression level, the more serious DNA DSBs degree [45]. So the Significantly and continuously elevated γ-H_2AX expression in G422 and GL261 cells reflects the presence of severe and unrepaired DNA DSBs. Additionally, Dbait molecules mimic DSBs, which activates DNA-PKCs and phosphorylate P53, thereby recruiting DNA damage repair proteins to the ends of Dbait molecules rather than the actual DNA damage sites. Thus, A2-CL/Dbait NPs primarily enhance radiation sensitivity by impairing the DNA damage repair mechanisms of GBM cells.

In vivo, radiosensitization therapy with Dbait significantly prolonged the survival time of mice compared to RT and RT + A2-CL. The impaired DNA damage repair induced by Dbait led to GBM cells death and enhanced the exposure of TDPAs. The release and presentation of TDPAs are crucial for boosting the tumor immune response, which can be amplified through a combination of radiotherapy and immunotherapy [46, 47]. In the CNS, radiotherapy disrupts the BBB, allowing immune mediators to penetrate the tumor region and transform the brain environment from an "immune-isolated compartment" to an "immunologically distinct" one [48, 49]. Consequently, the combination of RT and A2-CL/Dbait NPs further promoted cytokine secretion, CD8 + T cell differentiation as well as inhibited Treg cells, thereby enhancing the radiation associated antitumor immune effect.

Our research did not stop here, if all released TDPAs can be gathered, cancer immunity will be further improved. Therefore, based on previous experiment results [21, 22], the development of A2-PLGA-PEG-Mal NPs to capture and enrich TDPAs represented a significant step forward. In vitro experiment, we demonstrated that A2-PLGA-PEG-Mal NPs can significantly increase in size and capture TDPAs effectively when cocultured with them. The proteins adsorbed by PLGA-PEG-Mal were neoantigens (such as Actn4, Ap3d1 and etc.) and

damage associated molecular patterns (DAMPs) including H2afz, H3f3c etc. This enhances the presentation of TDPAs, potentially leading to a more robust immune response. Besides, by using PLGA-PEG-Mal NPs to adsorb tumor antigens in situ, we offered a practical solution to the problem of tumor heterogeneity. Instead of targeting individual tumor antigens, this approach allows for the enrichment of diverse neoantigens and DAMPs that are shared among tumors. This broadens the scope of the immune response and addresses the challenge of personalized immunotherapy. The use of "local materials" to capture and present TDPAs directly in the tumor environment enhances immune efficacy and avoids the complication associated with systemic antigen delivery and the variability of tumor antigens across patients.

All of the treatments involving radiation sensitization and TDPAs capture provided an excellent precondition for anti-OX40 antibodies application. OX40 is highly expressed on activated and memory T cells, as well as regulatory T cells (Tregs) [50]. The interaction of OX40 with anti-OX40 effectively "accelerates" the immune response by promoting T cell activation and proliferation. The use of anti-OX40 conjugated to NPs helps to significantly boost theimmune response against GBM cells. Ultimately, OS of GBM-bearing mice was significantly prolonged and tumor region in the brain was partially or completely regressed, which was consistent with previous studies [19, 51–53]. In vivo, we observed the obvious increase of CD8+T cells and decrease of Tregs in RT+A2-CL/Dbait+A2-PLGA-PEG-Mal/anti-OX40. This anti-cancer immune response is sustained and effective, verified by resistance against re-implantation of GL261 cells. In CD8+T cell depletion assay, the absence of survival benefit confirmed the anti-OX40-induced immune response was heavily reliant on T cells.

Overall, this study represents an innovative approach by integrating radiosensitization, TDPAs capture and immune agonists. It effectively addressed three critical challenges in GBM. This novel combination not only enhances the efficacy of GBM treatment but also provides valuable insights and strategies that could be applied to the comprehensive management of other tumors. The findings from this study could serve as a reference for developing more effective treatment paradigms in oncology.

Supplementary information

The online version contains supplementary material available at https://doi.org/10.1186/s13014-024-02511-9.

Supplementary Material 1

Supplementary Material 2

Supplementary Material 3

Supplementary Material 4

Supplementary Material 5

Supplementary Material 6

Supplementary Material 7

Author contributions

X.W. was responsible for conceptualization, data curation, formal analysis, investigation, methodology, software, visualization and writing original draft; ZY.S was responsible for data curation, formal analysis, supervision and review the manuscript; XT. C was responsible for data curation, formal analysis, methodology and visualization; HM.L was responsible for conceptualization and methodology; H.Q was responsible for conceptualization, methodology, supervision and review the manuscript; X.D was responsible for conceptualization, methodology, supervision and review the manuscript; DB.Q was responsible for MTT assays conduction and H.W was responsible for live/dead cell staining assay in revised manuscript; A.Z.W was responsible for conceptualization, methodology, supervision and review the manuscript; LZ.Z was responsible for conceptualization, funding acquisition, project administration, supervision and review the manuscript.All authors reviewed the manuscript.

Funding

This work was supported by Xuzhou special fund in scientific and technological innovation promotion (KC23266), National Natural Science Foundation of China (No. 81972845), and Specialist Team in Clinical Medicine of Xuzhou (No.2019TD003).

Data availability

No datasets were generated or analysed during the current study.

Declarations

Competing interests

The authors declare no competing interests.

Ethics approval and consent to participate

All animal research obtained ethical approval from Xuzhou Medical University (IACUC Issue No:202210S005). Approval of the research protocol by an Institutional Reviewer Board: N/A.

Consent for publication

N/A.

Registry and the Registration No. of the study/trial

N/A.

Author details

[1]Cancer Institute of Xuzhou Medical University, Xuzhou, Jiangsu, China
[2]Department of Radiation Oncology, Affiliated Hospital of Xuzhou Medical University, Kunpeng North Road No. 9, Xuzhou 221000, Jiangsu, China
[3]Department of Biomedical Engineering, Southern University of Science and Technology, 1088 Xueyuan Avenue, Shenzhen, Guangdong, China
[4]Department of Radiation Oncology, University of Texas Southwestern Medical Center, Dallas, TX, USA
[5]Jiangsu Center for the Collaboration and Innovation of Cancer Biotherapy, Jiangsu, China

Received: 3 June 2024 / Accepted: 21 August 2024
Published online: 12 September 2024

References

1. Alexander BM, Cloughesy TF. Adult glioblastoma. J Clin Oncol. 2017;35(21):2402–9.
2. van Tellingen O, et al. Overcoming the blood-brain tumor barrier for effective glioblastoma treatment. Drug Resist Updat. 2015;19:1–12.

3. Sampson JH, Maus MV, June CH. Immunotherapy for Brain tumors. J Clin Oncol. 2017;35(21):2450–6.
4. Hombach-Klonisch S, et al. Glioblastoma and chemoresistance to alkylating agents: involvement of apoptosis, autophagy, and unfolded protein response. Pharmacol Ther. 2018;184:13–41.
5. Biau J, et al. A preclinical study combining the DNA repair inhibitor dbait with radiotherapy for the treatment of melanoma. Neoplasia. 2014;16(10):835–44.
6. Quanz M, et al. Small-molecule drugs mimicking DNA damage: a new strategy for sensitizing tumors to radiotherapy. Clin Cancer Res. 2009;15(4):1308–16.
7. Liu N, et al. Improving radio-chemotherapy efficacy of prostate cancer by co-deliverying docetaxel and dbait with biodegradable nanoparticles. Artif Cells Nanomed Biotechnol. 2020;48(1):305–14.
8. Herath NI, et al. Potentiation of doxorubicin efficacy in hepatocellular carcinoma by the DNA repair inhibitor DT01 in preclinical models. Eur Radiol. 2017;27(10):4435–44.
9. Jiao X, et al. Dual-targeting and microenvironment-responsive micelles as a gene delivery system to improve the sensitivity of glioma to radiotherapy. Acta Pharm Sin B. 2019;9(2):381–96.
10. Liu H et al. Development of a hypoxic Radiosensitizer-Prodrug Liposome Delivery DNA repair inhibitor Dbait Combination with Radiotherapy for Glioma Therapy. Adv Healthc Mater, 2017. 6(12).
11. Yang ZZ, et al. Tumor-targeting dual peptides-modified cationic liposomes for delivery of siRNA and docetaxel to gliomas. Biomaterials. 2014;35(19):5226–39.
12. Karim R, et al. Nanocarriers for the treatment of glioblastoma multiforme: current state-of-the-art. J Control Release. 2016;227:23–37.
13. Pourgholi F, et al. Novel vehicles in treatment of Glioblastoma. Biomed Pharmacother. 2016;77:98–107.
14. Posadas I, Monteagudo S, Cena V. Nanoparticles for brain-specific drug and genetic material delivery, imaging and diagnosis. Nanomed (Lond). 2016;11(7):833–49.
15. Yan H, et al. Two-order targeted brain tumor imaging by using an optical/paramagnetic nanoprobe across the blood brain barrier. ACS Nano. 2012;6(1):410–20.
16. Oller-Salvia B, et al. Blood-brain barrier shuttle peptides: an emerging paradigm for brain delivery. Chem Soc Rev. 2016;45(17):4690–707.
17. Cho CF, et al. Blood-brain-barrier spheroids as an in vitro screening platform for brain-penetrating agents. Nat Commun. 2017;8:15623.
18. Gough MJ, Weinberg AD. OX40 (CD134) and OX40L. Adv Exp Med Biol. 2009;647:94–107.
19. Sagiv-Barfi I et al. Eradication of spontaneous malignancy by local immunotherapy. Sci Transl Med, 2018. 10(426).
20. Aspeslagh S, et al. Rationale for anti-OX40 cancer immunotherapy. Eur J Cancer. 2016;52:50–66.
21. Min Y, et al. Antigen-capturing nanoparticles improve the abscopal effect and cancer immunotherapy. Nat Nanotechnol. 2017;12(9):877–82.
22. Mi Y, et al. A dual immunotherapy nanoparticle improves T-Cell activation and Cancer immunotherapy. Adv Mater. 2018;30(25):e1706098.
23. Yuan Z, et al. Inhibition of glioma growth by a GOLPH3 siRNA-loaded cationic liposomes. J Neurooncol. 2018;140(2):249–60.
24. Yao H, et al. Nanoparticle formulation of small DNA molecules, Dbait, improves the sensitivity of hormone-independent prostate cancer to radiotherapy. Nanomedicine. 2016;12(8):2261–71.
25. Hoyle CE, Lowe AB, Bowman CN. Thiol-click chemistry: a multifaceted toolbox for small molecule and polymer synthesis. Chem Soc Rev. 2010;39(4):1355–87.
26. Zhang T, et al. Fluorinated Oligoethylenimine nanoassemblies for efficient siRNA-Mediated gene silencing in serum-containing media by effective endosomal escape. Nano Lett. 2018;18(10):6301–11.
27. Wen X, et al. Pulsed low-dose rate radiotherapy has an improved therapeutic effect on abdominal and pelvic malignancies. J Zhejiang Univ Sci B. 2021;22(9):774–81.
28. Awuah WA, et al. Exploring the role of Nrf2 signaling in glioblastoma multiforme. Discov Oncol. 2022;13(1):94.
29. Kanderi T, Gupta V. Glioblastoma Multiforme, in StatPearls. Treasure Island (FL); 2022.
30. Cloughesy TF, et al. Neoadjuvant anti-PD-1 immunotherapy promotes a survival benefit with intratumoral and systemic immune responses in recurrent glioblastoma. Nat Med. 2019;25(3):477–86.
31. Furtak J, et al. Survival after reoperation for recurrent glioblastoma multiforme: a prospective study. Surg Oncol. 2022;42:101771.
32. Liauw SL, Connell PP, Weichselbaum RR. New paradigms and future challenges in radiation oncology: an update of biological targets and technology. Sci Transl Med. 2013;5(173):173sr2.
33. Seung SK, et al. Phase 1 study of stereotactic body radiotherapy and interleukin-2–tumor and immunological responses. Sci Transl Med. 2012;4(137):137ra74.
34. Damiano V, et al. Cooperative Antitumor effect of multitargeted kinase inhibitor ZD6474 and ionizing radiation in glioblastoma. Clin Cancer Res. 2005;11(15):5639–44.
35. Quanz M, et al. Hyperactivation of DNA-PK by double-strand break mimicking molecules disorganizes DNA damage response. PLoS ONE. 2009;4(7):e6298.
36. Devun F, et al. Preclinical study of the DNA repair inhibitor Dbait in combination with chemotherapy in colorectal cancer. J Gastroenterol. 2012;47(3):266–75.
37. Chen M, et al. Targeted delivery of Dbait by an artificial extracellular vesicle for improved radiotherapy sensitivity of esophageal cancer. Am J Cancer Res. 2023;13(1):105–17.
38. Li S, et al. Angiopep-2 modified Cationic lipid-poly-lactic-co-glycolic acid delivery temozolomide and DNA repair inhibitor dbait to Achieve Synergetic Chemo-Radiotherapy against Glioma. J Nanosci Nanotechnol. 2019;19(12):7539–45.
39. Biau J, et al. Combining the DNA repair inhibitor Dbait with Radiotherapy for the treatment of high Grade Glioma: efficacy and protein biomarkers of resistance in preclinical models. Front Oncol. 2019;9:549.
40. Le Tourneau C, et al. First-in-human phase I study of the DNA-repair inhibitor DT01 in combination with radiotherapy in patients with skin metastases from melanoma. Br J Cancer. 2016;114(11):1199–205.
41. Dowdy SF. Overcoming cellular barriers for RNA therapeutics. Nat Biotechnol. 2017;35(3):222–9.
42. Kulkarni JA, Cullis PR. Meel, lipid nanoparticles enabling gene therapies: from concepts to clinical utility. Nucleic Acid Ther. 2018;28(3):146–57. van der.
43. Davis ME, et al. Evidence of RNAi in humans from systemically administered siRNA via targeted nanoparticles. Nature. 2010;464(7291):1067–70.
44. Li XY, et al. Multifunctional liposomes loaded with paclitaxel and artemether for treatment of invasive brain glioma. Biomaterials. 2014;35(21):5591–604.
45. Lobrich M, et al. gammaH2AX foci analysis for monitoring DNA double-strand break repair: strengths, limitations and optimization. Cell Cycle. 2010;9(4):662–9.
46. Wang Y, et al. The reciprocity between Radiotherapy and Cancer Immunotherapy. Clin Cancer Res. 2019;25(6):1709–17.
47. Weichselbaum RR, et al. Radiotherapy and immunotherapy: a beneficial liaison? Nat Rev Clin Oncol. 2017;14(6):365–79.
48. Di Giacomo AM, et al. Immunotherapy of brain metastases: breaking a dogma. J Exp Clin Cancer Res. 2019;38(1):419.
49. Hormuth DA 2, et al. Opportunities for improving brain cancer treatment outcomes through imaging-based mathematical modeling of the delivery of radiotherapy and immunotherapy. Adv Drug Deliv Rev. 2022;187:114367.
50. Imianowski CJ et al. IFN-gamma production by functionally reprogrammed Treg cells promotes anti-tumor efficacy of OX40/CD137 bispecific agonist therapy. Cancer Res Commun, 2024.
51. Morris A, et al. Induction of anti-mammary cancer immunity by engaging the OX-40 receptor in vivo. Breast Cancer Res Treat. 2001;67(1):71–80.
52. Petty JK, et al. Survival in human colorectal cancer correlates with expression of the T-cell costimulatory molecule OX-40 (CD134). Am J Surg. 2002;183(5):512–8.
53. Lu X. OX40 and OX40L Interaction in Cancer. Curr Med Chem. 2021;28(28):5659–73.

Publisher's note